


## RESEARCH ARTICLE

# Computational study of novel pentacene derivatives: Prediction of structural, electronic, and optical properties

Salvatore Petralia | Giuseppe Forte Department of Drug Science and Health,  
University of Catania, Catania, Italy**Correspondence**Giuseppe Forte, Department of Drug  
Science and Health University of Catania,  
Via S. Sofia 64, Catania 95125, Italy.  
Email: [gforte@unict.it](mailto:gforte@unict.it)**Funding information**

University of Catania

**Abstract**

Several properties of a series of novel disubstituted pentacenes, in which the substituents are donor and acceptor groups, were investigated by using the ab initio methods. In particular, the role of different substitution positions for acceptor group was explored. Calculations predict that pentacene derivatives were highly soluble and oxidatively stable than the unsubstituted pentacene. Simulated absorption spectra show that 9-nitropentacen-2-amine (**PD2**) exhibits three absorption bands in the ultraviolet and visible regions. In general, substituents have important impact on the first hyperpolarizability value, and a remarkable enhancement of static second hyperpolarizability is revealed in this study; however, further investigations are required to confirm this finding. Molecular dynamics simulations of the solid state suggest that a material based on 9-nitropentacen-2-amine and 10-nitropentacen-2-amine could exhibit low resistivity due to the potential amount of  $\pi$ - $\pi$  stacking. The results emphasize the potential of using the herein studied pentacene-based compounds, with particular reference to **PD2**, for future applications in the optoelectronic and photonic fields.

**KEYWORDS**

ab initio, GAP, NLO properties, Pentacene, UV/VIS spectra, withdrawing group

**1 | INTRODUCTION**

In the last few decades, organic compounds and in general carbon-based materials have fascinated great interest because of their capabilities to fabricate low-cost multifunctional and flexible devices. This has determined the development of organic materials with potential applications in the fields of microelectronics as well as optoelectronics.<sup>[1-7]</sup> The versatility of organic materials has expanded the technological interest in many different applications based on devices such as organic light-emitting diodes,<sup>[8]</sup> organic field-effect transistors (OFET),

organic photovoltaic cells, and transistors.<sup>[9-13]</sup> In the electronic field, the use of OFET memory device benefit from their high compatibility with different substrates, easy to integrate structure, and nondestructive readout capabilities.<sup>[8]</sup> OFET are constructed primarily according to the principle of the thin-film transistor, and a large number of studies have investigated on the acene and heteroacene-based organic semiconductor for OFET.<sup>[14]</sup>

Carbon-based nanomaterials such as polymer dots, aromatic quantum dots, organic coating, and their metal/inorganic hybrid derivatives are fascinating materials since their interesting optical, electrical, and photothermal

This is an open access article under the terms of the [Creative Commons Attribution](https://creativecommons.org/licenses/by/4.0/) License, which permits use, distribution and reproduction in any medium, provided the original work is properly cited.

© 2022 The Authors. *Journal of Physical Organic Chemistry* published by John Wiley & Sons Ltd.

properties. They are largely utilized for the fabrication of nanosized smart devices for biomedical application such drug and gene delivery system<sup>[15,16]</sup> and biosensing.<sup>[17,18]</sup>

Pentacene and its derivatives are reported to have a very high carrier mobility<sup>[19,20]</sup>; however, it has many drawbacks. In fact, it is insoluble in water, poorly soluble in common organic solvents, undergoes photo-oxidation at 6 and 13 positions when exposed to light and oxygen,<sup>[21]</sup> and known to crystallize in herringbone arrangement, characterized by a minimal  $\pi$  stacking.<sup>[22]</sup> This order results in a poor dispersion of the electronic bands limiting the transport properties. Several different pentacene polytypes exist, differ slightly in their crystal packing, and exhibit a band gap energy within the range 1.9 to 2.2 eV.<sup>[23–25]</sup>

To overcome these inherent limits, numerous derivatives have been synthesized. Okamoto et al. have prepared symmetric and asymmetric derivatives with electron-withdrawing (e.g., Cl, Br, CN, and  $\text{CF}_3$ ) groups in positions 2, 3, 9, and 10 that obtain compounds more oxidatively stable than pentacene due to the lowering of the highest-occupied molecular orbital (HOMO)–lowest-unoccupied molecular orbital (LUMO) gap.<sup>[14,26]</sup> Soluble pentacene precursor was prepared by attaching via Diels Alder reaction of N-sulfinylamide to the 6,13 positions obtaining a very air-stable product that is highly soluble in chlorinated hydrocarbons.<sup>[27]</sup> Highly alkyl-substituted pentacene derivatives have been synthesized with a general method obtaining compounds soluble in many organic solvents<sup>[28]</sup>; in general, methodologies for the synthesis of pentacene and its derivatives have been reported in a review of Bhatia et al.<sup>[29]</sup> Anthony et al. have functionalized pentacene obtaining a compound highly soluble in the common organic solvents; moreover, the derivative showed a very different crystal packing compared with unsubstituted pentacene; in fact, the herringbone pattern was disrupted in favor of a two-dimensional  $\pi$ -stacked array, and an intermolecular orbital overlap was enhanced.<sup>[30]</sup> The new order in the solid state reduced drastically the interplanar spacing of the aromatic rings to 3.47 Å (6.27 Å was estimated for unsubstituted compound) giving rise to a significant conductivity enhancement. A lower interplane distance, 3.41 Å, was achieved attaching a bulky group to pentacene by means of a rigid alkyne spacer; such strategy favored the face-to-face interactions with respect to the edge-to-face; moreover, the derivatives possessed resistivities much lower than that measured in crystals of pentacene.<sup>[31]</sup> A  $\pi$ - $\pi$  stacking distance of 3.08 Å was measured in strained TIPS–pentacene thin film, increasing the hole mobility up to 4.6  $\text{cm}^2 \text{V}^{-1} \text{s}^{-1}$ .<sup>[32]</sup>

Large optical nonlinearity of pentacene films, pentacene dimers, pentacene/ITO thin film, and pentacene-doped derivatives have been also observed; in particular,

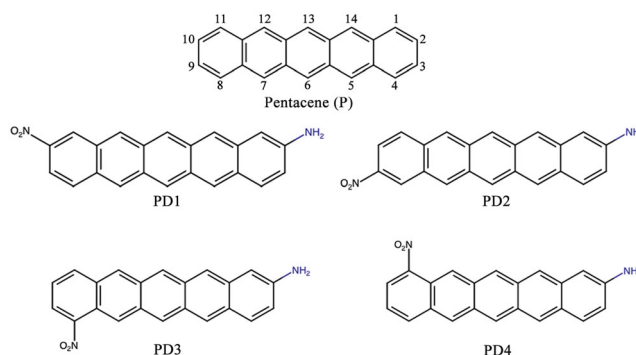


**FIGURE 1** Chemical structures of pentacene derivatives **PD1–PD4**

they result particularly interesting because their large second hyperpolarizabilities  $\gamma$  (third-order nonlinear optical property) and their fast and low timescales response. Due to these remarkable characteristics, pentacene films have wide application in advanced optoelectronic and photonic devices.<sup>[33–40]</sup>

In this paper, we report a computational study of new pentacene derivatives with the electron-withdrawing nitro group substituted at the 8, 9, 10, and 11 positions and the donor amine group substituted to the 2-position, see Figure 1. We analyzed the role of different substitution positions for  $-\text{NO}_2$  in tuning the electronic and optical properties, and comparing them with unsubstituted pentacene, we demonstrate that substituents broaden the absorption spectra and enhance the NLO properties. Herein, we also predict the solubility of **PD1–PD4** derivatives in different organic solvents and their capability to prevent photodegradation through singlet oxygen sensitization.

Finally, the role of the substituents on the crystalline order is investigated; a partial disruption of the edge-to-face interactions is observed, in particular for **PD2**, leading to a more efficient  $\pi$  overlap between each stack and, as a consequence, a reduction in resistivity for this structure.

It is expected that the investigation of interplane distance, NLO, absorption UV/VIS, and solubility in organic solvent for the herein studied compounds can give profound insight into the effect of terminal substituents on the pentacene performance and assist the design of a more efficient material for application in photonic and optoelectronic fields.

## 2 | METHODS

The geometries of pentacene and its derivatives were fully optimized in the framework of the density-functional theory (DFT) with the hybrid B3LYP

functional and the 6-311 + G(2d,p) basis set; the reason of this choice lies in the fact that calculated B3LYP HOMO–LUMO gap of pentacene in solution is in excellent agreement with experimental value.<sup>[16,21,41–43]</sup> The optimized geometries were used to compute solvation energy,  $\Delta G_{solv}$ , which allow to predict the relative solubility in different environments. Such calculations were performed with a parametrized solvation model, SMD, developed specifically to predict free energy of solvation.<sup>[44]</sup>  $\Delta G_{solv}$  were obtained by difference of the Gibbs free energy, derived from the frequency calculations, between the gas phase and the solution. UV/VIS spectra were investigated within the time-dependent DFT approach adopting the Coulomb attenuating method-B3LYP functional, (CAM-B3LYP), a long-range corrected version of B3LYP, which predicts excitation energy values very close to experimental data.<sup>[45–47]</sup> The SMD method was also adopted to model the solvation effect. Vibrational coupling was considered at the Franck–Condon level adopting the full Duschinsky formalism.

To estimate the nonlinear optical properties  $\alpha$  and  $\beta$  at quantitative accuracy level of approximation, the extended basis set 6-311 + G(3df,3pd) has been employed. The polarizability  $\alpha$  is a symmetric matrix, here is reported the isotropically averaged polarizabilities  $\langle\alpha\rangle$  defined as

$$\langle\alpha\rangle = \frac{\alpha_{xx} + \alpha_{yy} + \alpha_{zz}}{3} \quad (1)$$

The first-order hyperpolarizability  $\beta$  is described by a  $3 \times 3 \times 3$  matrix, and its magnitude is defined as

$$\beta_{tot} = \sqrt{\beta_x^2 + \beta_y^2 + \beta_z^2} \quad (2)$$

where  $\beta_i$  is given by

$$\beta_i = \frac{\sum_j (\beta_{ijj} + \beta_{jji} + \beta_{jjj})}{3} \quad i, j = (x, y, z)$$

It is known that DFT functionals overestimate nonlinear optical properties for systems with significant electron delocalization; nevertheless, CAM-B3LYP improve many of the shortcomings of most functionals.<sup>[48,49]</sup> The quantum chemical calculations were performed using the Gaussian 16 program.<sup>[50]</sup>

The initial structures for molecular dynamics (MD) simulations were built by the replacement of hydrogen atoms of the bulk triclinic crystal of pentacene (unit cell parameters:  $a = 5.959$ ,  $b = 7.596$ ,  $c = 15.6096$ ,  $\alpha = 81.25$ ,  $\beta = 86.56$ ,  $\gamma = 89.80$ )<sup>[51]</sup> with nitro and amine groups. The unit cells were replicated  $2 \times 2 \times 2$  along the  $a b c$  directions so that the dimensions of the final supercell were  $1.19 \times 1.52 \times 3.12$  nm, see Figure 2. An equilibrium protocol consisting of 3000 iterations of geometry optimization with CVFF parametrization,<sup>[52,53]</sup> followed by 200-ns MD simulation was applied to each compound. The evidence that the systems were equilibrated was provided by the root mean square deviation; afterwards, MD simulation was carried out for further 200 ns, and collected data were considered for analysis. The simulations were run under periodic boundary

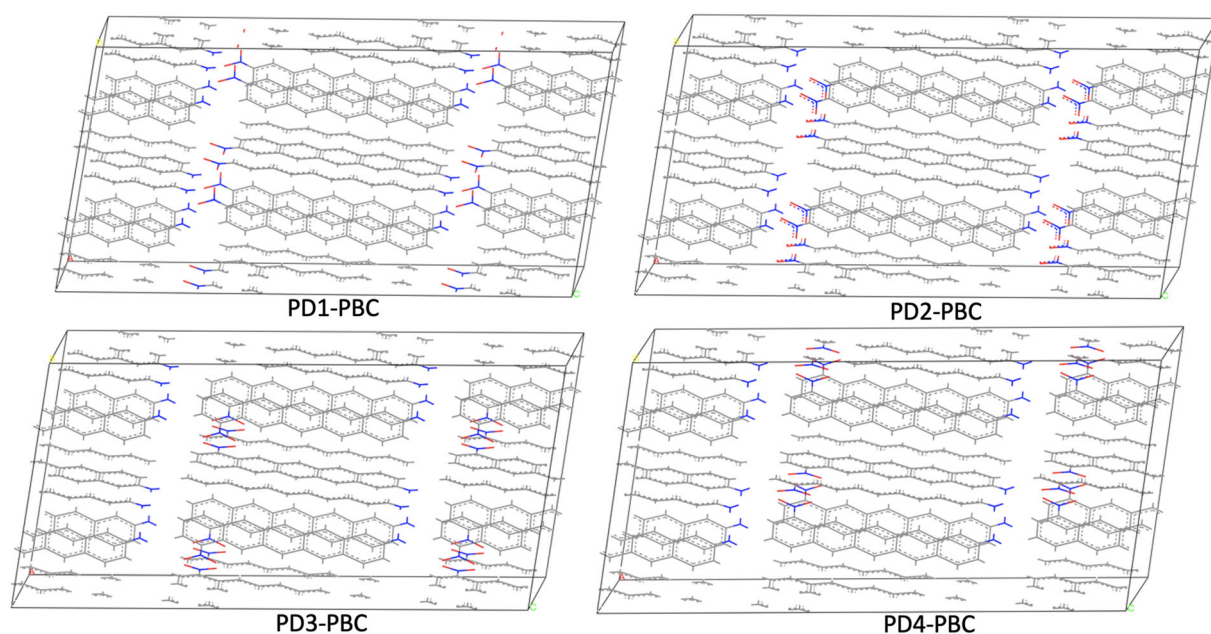


FIGURE 2 Supercells simulated in molecular dynamics

TABLE 1  $\Delta G_{\text{soln}}$  (kcal mol<sup>-1</sup>) values of pentacene (P) and PD1–PD4 in different solvents

Environment	P	PD1	PD2	PD3	PD4
Cyclohexane	-13.83	-15.87	-16.10	-15.63	-15.93
Chloroform	-16.72	-20.57	-20.64	-20.22	-20.45
THF	-14.54	-19.70	-19.99	-19.38	-19.56
Ethanol	-13.42	-18.87	-18.89	-18.41	-18.48

conditions in NPT ensemble at  $P = 1$  atm controlled by the Berendsen barostat (decay constant saw set to 0.1 ps) and  $T = 298$  K maintained with the Nose thermostat ( $Q$  ratio = 0.01). A time step = 1 fs was employed to integrate the equation of motion, the Ewald summation was applied for electrostatic and VdW interactions with a cut-off distance of 1.5 nm. Material Studio 2017 was used to prepare the initial structures and the Forcite module was adopted for MD simulations.<sup>[54]</sup>

### 3 | RESULTS AND DISCUSSION

#### 3.1 | Solubility and photostability

The optimized geometries provided no imaginary frequency values, thus confirming the represented local energy minima, see Supporting information S1. In order to predict the solubility of the derivatives in different solvents, we have calculated the free energy of solvation,  $\Delta G_{\text{soln}}$ , following the procedure discussed in Section 2. From the results reported in Table 1, it turns out that PD1–PD4 are expected to have higher solubility in solvent compared with unsubstituted pentacene P; it is found that PD2 shows the highest solubility in the solvents here considered exhibiting a maximum value of  $-20.64$  kcal mol<sup>-1</sup> in chloroform. In view of this characteristics, the system consisting of PD2 in chloroform will be considered as a reference for this study.

Energy gaps between HOMO and LUMO levels calculated at B3LYP/6-311 + G(2d,p) for both the gas phase and chloroform solvent are reported in Figure 3. As discussed above, the band gap value of pentacene in the solution is very close to the experimental values.<sup>[41]</sup>

Comparison in chloroform shows a notable difference of the calculated band gap values, which are found between 0.35–0.37 eV. Figure 3 clearly shows that such difference can be mainly due to the lowering of the LUMO level in the derivatives whereas slight differences are observed in the HOMO levels. Such findings are in line with the results found by Maliakal et al.'s<sup>[21]</sup> study on 6-13 substituted pentacene; we therefore consistently predict that solutions of PD1–PD4 could exhibit an excellent photostability due to the high stabilization of the

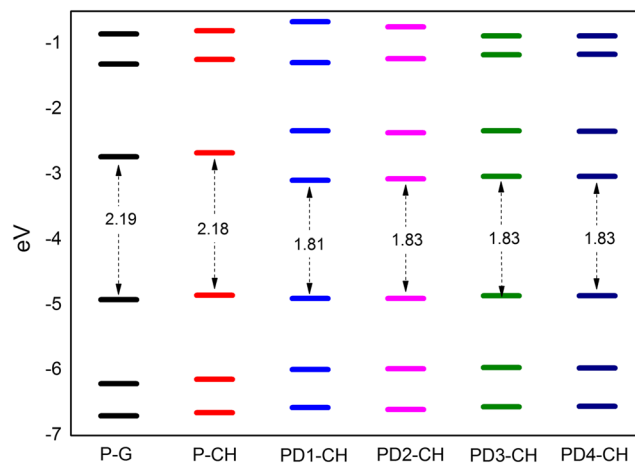


FIGURE 3 Selected computed energy levels, highest-occupied molecular orbital, lowest-unoccupied molecular orbital, band gap values of pentacene (P), and derivatives (G = gas phase, CH = chloroform)

LUMO energy level. Following the conclusions reported in Maliakal et al.,<sup>[21]</sup> we have also computed the relaxed triplet excitation energies for pentacene and PD2 in chloroform and have found 0.79 and 0.26 eV, respectively. The triplet excitation energy for PD2 is much lower than the energy difference between ground state and singlet oxygen molecule (0.98 eV), indicating that photodegradation due to singlet sensitization should be prevented.

#### 3.2 | UV/VIS absorption spectra and NLO properties

The absorption spectra have been calculated by using CAM-B3LYP functional as the results obtained in the simulation of the UV/VIS spectra of pentacene in the gas phase are in excellent agreement with experimental data.<sup>[43]</sup> Indeed, we have found that the vertical excitation energies of the first excited state and the main transition are respectively 2.26 eV and 4.55 eV (see Halasinski et al.<sup>[43]</sup> for comparison). The main electronic transitions ( $f_{\text{calc}} > 0.2$ ), calculated in chloroform, are shown in Table 2; the overall data relating to the other solvents are reported in Table S1.

**TABLE 2** In the second column are reported the main contributions to the transitions. Energy values and oscillator strength,  $f$ , are reported in the other columns

Compound	Main contribution to the transition	Energy (eV)	$f_{\text{calc}}$
PD1	H $\rightarrow$ L	2.014	0.094
	H $\rightarrow$ L + 1	2.932	0.647
	H-2 $\rightarrow$ L	3.694	1.152
	H $\rightarrow$ L + 2	3.775	1.296
	H $\rightarrow$ L + 3	4.100	0.714
PD2	H $\rightarrow$ L	2.030	0.195
	H-1 $\rightarrow$ L	3.357	1.857
	H $\rightarrow$ L + 3	4.089	1.632
	H $\rightarrow$ L + 3	4.351	0.500
PD3	H $\rightarrow$ L	2.040	0.136
	H $\rightarrow$ L + 2	3.770	0.835
	H-2 $\rightarrow$ L	3.905	1.932
	H $\rightarrow$ L + 3	4.034	1.030
PD4	H $\rightarrow$ L	2.034	0.181
	H-1 $\rightarrow$ L	3.300	0.446
	H $\rightarrow$ L + 2	3.796	0.403
	H $\rightarrow$ L + 3	3.914	1.759
	H $\rightarrow$ L + 3	4.029	1.285

The excitation to the first excited state mainly consists of  $n \rightarrow \pi^*$  transition, exhibits a small value of the oscillator strength  $f$ , and is characterized by the promotion of an electron from HOMO (H) to LUMO (L), see Table 2 and Figure 4.

On the other hand, the  $\pi \rightarrow \pi^*$  principal transitions, for example, the highest value of  $f_{\text{calc}}$ , involve several molecular orbitals, and the related excitation energies are found between 3.357 and 3.914 eV, see Table S1. The differences of dipole moment between the ground state and the excited states reveal that excited states of the studied compounds are more polar as compared with ground state; hence, a significant redshift due to the stabilization of the excited state is observed as the solvent polarity increases, see Table 3.

Interestingly, **PD2** is the only compound that absorbs with almost the same intensity at two different wavelengths, around 300 and 400 nm; in addition, it shows a further absorption in the visible region at higher intensity than the unsubstituted pentacene and other derivatives, see Figure 5. The 0–0 transition of the vibrationally resolved absorption spectra is found at 610 nm (see the inset in Figure 5), about 45-nm redshifted compared with the unsubstituted pentacene in chloroform.

All the compounds here studied have the requisite properties for second-order nonlinear behavior because they are characterized by an extensive electron

delocalization and possess a large difference between ground and excited state dipole moment and a considerable transition state dipole moment.

The calculated values of polarizability ( $\alpha$ ) in chloroform reveal that compared with the unsubstituted pentacene ( $\alpha = 445.03$ ), the values of the derivatives are slightly enhanced (see Table 4) whereas the calculated values of the other properties show a significant increase.

The values of  $\beta_{\text{tot}}$  reported in Table 4 reveal a trend that is related to the magnitude of the ground state dipole moment reported in Table 3. To better explain the difference in the calculated values, the following two-level expression of  $\beta_{\text{xxx}}$  was used:

$$\beta_{\text{xxx}} \propto \frac{\Delta\mu^x \cdot f^x}{\Delta E^3} \quad (3)$$

where  $\beta_{\text{xxx}}$  is assumed to be the component dominated by ground state and one crucial transition state (CTS),  $\Delta\mu^x$  is the difference of dipole moment between the ground state and the CTS,  $f^x$  is the  $x$  component of oscillator strength, and  $\Delta E$  is the transition energy.<sup>[56]</sup> Taking into account the critical transition states of **PD1–PD4**, it was found that both  $\Delta\mu$  and  $f$  dominate the increasing order of the  $\beta_{\text{tot}}$  values; in particular, a much larger value of  $f$  is at the base of the difference between **PD2** and **PD1** while  $\Delta\mu$  prevails in the comparison between **PD3** and **PD4**.

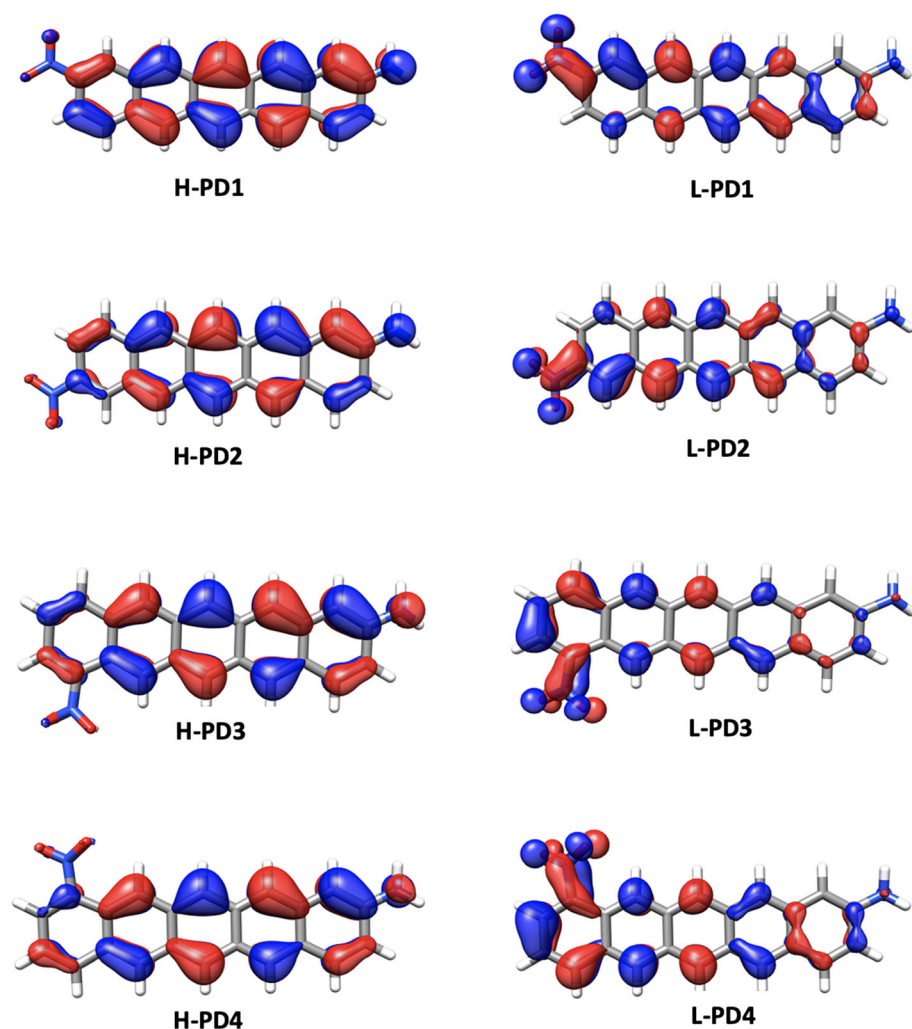


FIGURE 4 H and L of compounds PD1–PD4. Nonbonding electrons pair are on the aminic nitrogen distinguish highest-occupied molecular orbitals

TABLE 3 PD1–PD4 dipole moment values (Debye) of the ground state (GS) and the first excited state (ES) in different environment

Environment	PD1-GS	PD1-ES	PD2-GS	PD2-ES	PD3-GS	PD3-ES	PD4-GS	PD4-ES
Cyclohexane	10.45	17.56	10.68	17.83	7.62	14.31	7.53	13.72
Chloroform	11.34	19.67	11.64	20.20	8.22	15.63	8.27	15.16
THF	11.43	19.69	11.71	20.23	8.29	15.62	8.40	15.04
Ethanol	12.42	22.53	12.83	23.46	9.01	17.43	9.24	17.09
Gas	9.507	14.929	9.316	15.057	6.832	12.398	6.664	11.807

The second hyperpolarizability ( $\gamma$ ) values are also reported in Table 4 and were computed with an incident light corresponding to the maximum absorption in the UV/VIS region. Here we report the total magnitude of  $\gamma$  measured as

$$\gamma_{tot} = \sqrt{\gamma_x^2 + \gamma_y^2 + \gamma_z^2} \quad (4)$$

where  $\gamma_i$  is given by

$$\gamma_i = \frac{\sum_j (\gamma_{ijji} + \gamma_{ijjj} + \gamma_{ijjj})}{15} \quad i, j = (x, y, z)$$

All compounds exhibit a  $\gamma$  value larger than pure pentacene ( $\gamma = 2.617 \cdot 10^5$  a.u.), and the values follow the same trend observed for  $\beta$ . However, it should be emphasized that to estimate this property at quantitative accuracy level, an extended basis set is required with a consequent high computational cost. Herein, the

**FIGURE 5** Simulated UV/VIS absorption of pentacene and derivatives in chloroform: in the inset, the vibrationally resolved absorption spectra are pictured. The spectra are Gaussianbroadened with 0.3 eV (half width half maximum).

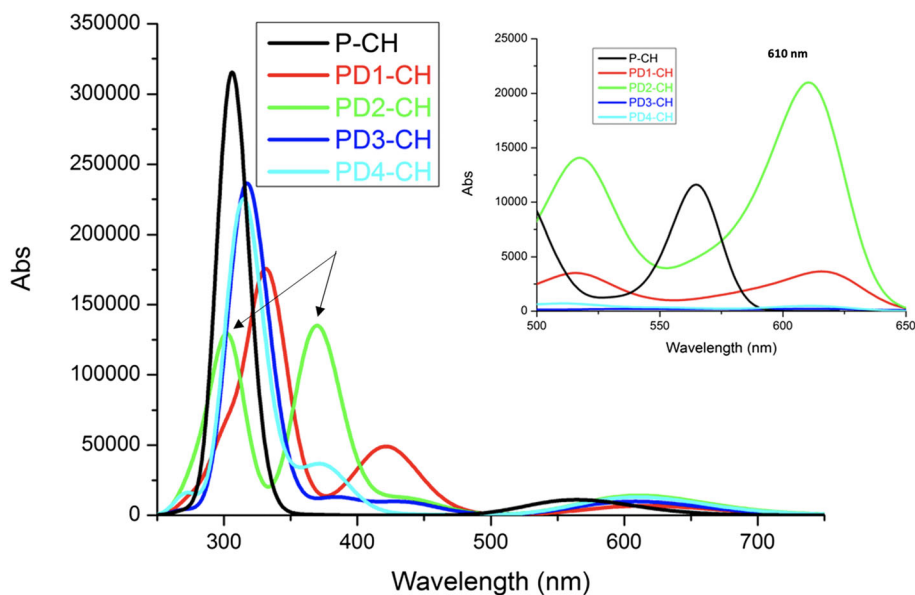


**TABLE 4** The values were calculated using the Multiwfn 3.8 program<sup>[55]</sup>

Compound	$\alpha$ (a.u.)	$\beta_{tot}$ (a.u.)/10 <sup>4</sup>	$\Delta E$ (eV)	$\Delta\mu^x$ (a.u.)	$f^x$	$\Delta\mu \cdot f/\Delta E^3$ (a.u.)/10 <sup>3</sup>	$\gamma_{tot}^*$ (a.u.)/10 <sup>6</sup>
PD1	526.181	2.693	2.932	5.393	0.761	3.281	1.607
PD2	536.550	4.022	3.357	4.305	1.775	4.072	2.857
PD3	506.716	1.495	3.905	1.427	2.058	0.994	0.961
PD4	510.971	1.959	3.919	1.860	1.888	1.180	1.378

calculations were carried out at the 6-311(d) level; therefore, the values reported cannot be considered for the purposes of a rigorous estimate. In this context, our aim is to highlight the potential high value of  $\gamma$  on which authors intend to further investigate.

### 3.3 | MD simulations

As discussed in Section 1, the  $\pi$ - $\pi$  stacking distance greatly influence the orbital overlap and, as a consequence, the mobility. The herringbone packing of pentacene is characterized by a minimal  $\pi$  stacking (see Figure 6); hence, an MD study in the solid state was performed to evaluate the role of the substituents on the separation between distance plane, for example,  $\pi$  stacking.

To this purpose, MD simulations on the systems represented in Figure 6 were performed at room temperature focusing on the arrangement between the planes which can promote the face-to-face interactions. During the simulations, the cell parameters were optimized, and as expected, an increasing of the supercell volume was observed in all cases compared with the initial value. To investigate on the plane interactions, was considered the average value of an index of planarity,  $I_p$ , measured

during the production phase. With reference to Figure 6 right such index measures the dihedral angle between two adjacent molecules, hence we have evaluated the average value  $I_{p_{av}}$  defined as follow:

$$I_{p_{av}} = \frac{\sum_{i=1}^{n=\text{adjacent planes}} I_{p_i}}{n}$$

Data shown in Figure 7 indicate that  $I_{p_{av}}$  decreases significantly from the initial value of 42.34° in **PD1** and **PD2** derivatives whereas an increasing of such index is observed during MD simulations of **PD3** and **PD4**. These findings suggest that for **PD1** and **PD2**, the planes tend to become parallel causing the disruption of the herringbone packing and, potentially, the promoting of the  $\pi$ - $\pi$  interactions between the planes, which affects electron orbital overlap and charge mobility. In particular, 10-nitropentacen-2-amine, **PD1**, is expected to exhibit higher carrier mobility, compared with unsubstituted pentacene, due to the lower value of  $I_{p_{av}}$ , snapshots of the simulated structures after 200-ns MD are reported in two different views, in Supporting information S1. By contrast, an increase of the resistivity is expected for both **PD4** and, in particular, **PD3** because the substitution of

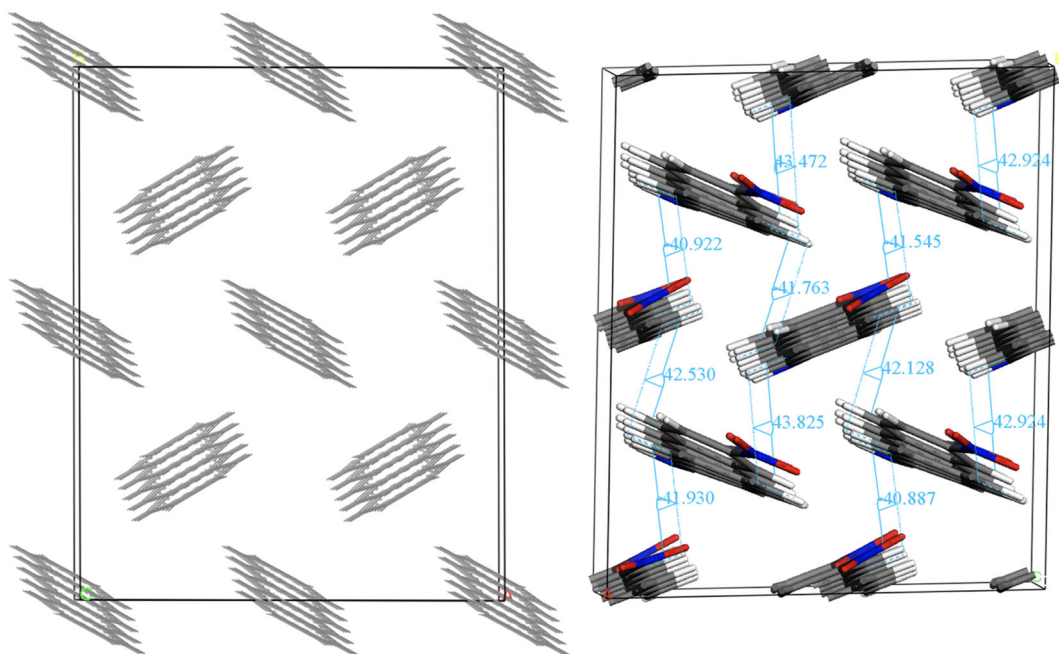


**FIGURE 6** Solid state order of unsubstituted pentacene (left); initial configuration for MD simulations (the case of **PD2** is shown) and dihedral angle initial values between adjacent planes (right)

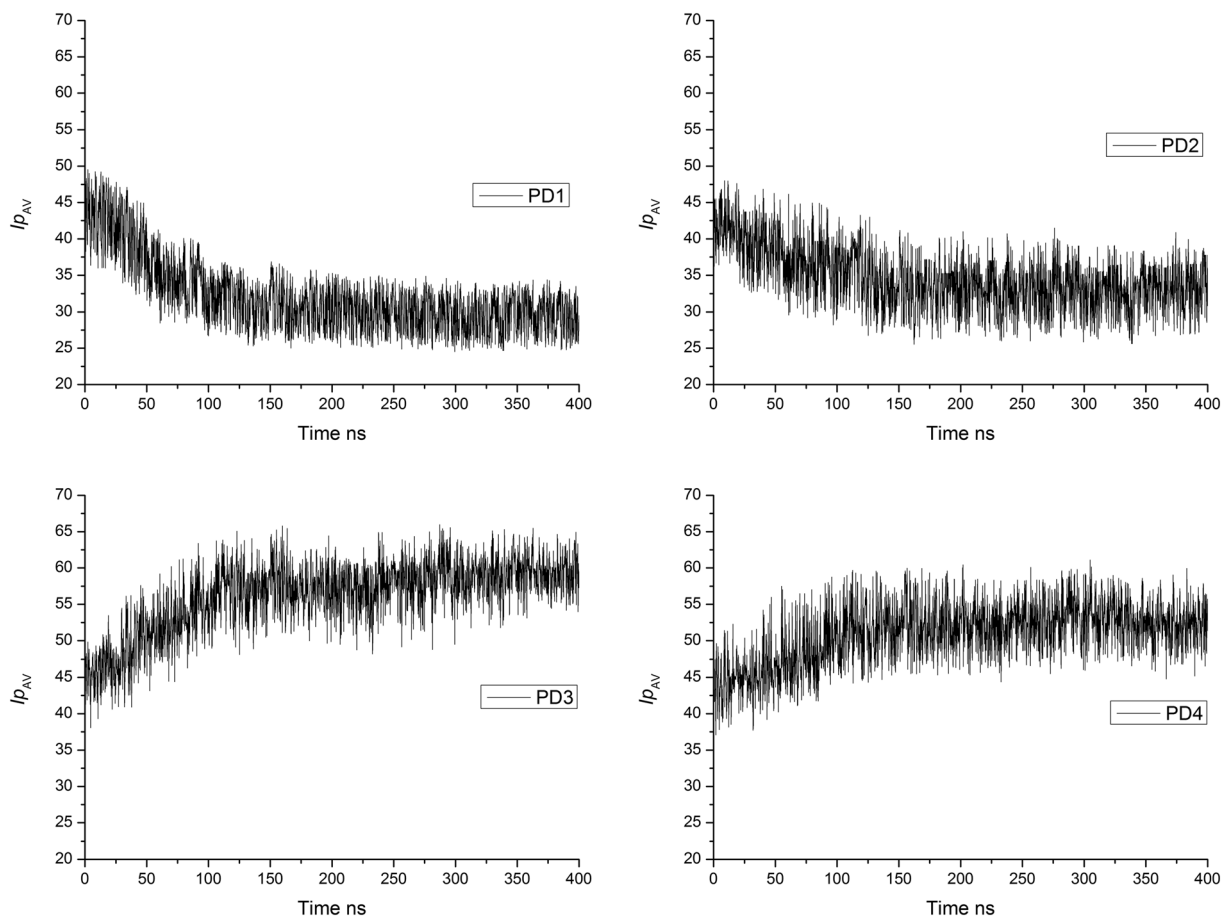


**FIGURE 7** Fluctuation of  $I_{p_{av}}$  over time for **PD1–PD4**



nitro group in positions 8 or 11 enhances the dihedral angle between adjacent planes, see Supporting information S1.

In conclusion, a different substitution position of the nitro group plays a significant role in the crystal packing; indeed, the large values of the dipole moment showed by **PD1** and **PD2** can explain the more effective interaction between two adjacent planes (molecules). On the other hand, in **PD3** and **PD4**, the steric hindrance due to the presence of hydrogen atoms in positions 7 and 12 determines the loss of planarity of the nitro group influencing the interplane interactions.

## 4 | CONCLUSIONS

We have systematically investigated electronic and optical properties of new pentacene-based compounds by using DFT and TDDFT approaches. These derivatives consist of amine group introduced in the 2-position as electronic donor and nitro group added in 8, 9, 10, 11 positions as acceptor. Properties were found to be tuned by changing the position of the acceptor group, in particular 9-nitropentacen-2-amine (**PD2**) shows the most promising properties for optoelectronic and photonic applications. Results predict an increase in the solubility of the derivatives in various solvents, mainly in chloroform, compared to unsubstituted pentacene, and a great photostability preventing singlet oxygen sensitization. All the derivatives exhibit redshift due to the increase of the excitation state dipole moment; in particular, **PD2** significantly absorbs energy at about 300, 400, and 600 nm. All the compounds possess considerable values of the first hyperpolarizabilities, which arose from the difference of dipole moment and oscillator strength between the ground state and crucial transition state. A potential large value of the second polarizability is predicted, but further investigations with more extended basis set are requested. Finally, MD studies of bulk structure indicate that nitro groups added in positions 9 and 10 tend to decrease the dihedral angle values between adjacent planes thus favoring the  $\pi$ - $\pi$  stacking with potential enhancing of the charge transport. In consideration of the discussed properties, with particular reference to **PD2**, authors expect that this work will contribute to design new devices with potential applications in the optoelectronic and photonic fields.

## ACKNOWLEDGMENTS

This research was partially funded by the University of Catania (*Piano della Ricerca di Ateneo, Linea di Intervento 2*, 2018–2020 and PIACERI—GRABIO project). Open Access Funding provided by Università degli Studi di Catania within the CRUI-CARE Agreement.

## ORCID

Giuseppe Forte  <https://orcid.org/0000-0002-6607-6038>

## REFERENCES

- [1] C. L. Wang, H. L. Dong, W. P. Hu, Y. Q. Liu, D. B. Zhu, *Chem. Rev.* **2012**, *112*, 2208.
- [2] M. Yi, Y. Guo, J. Guo, T. Yang, Y. Chai, Q. Fan, L. Xie, W. Huang, *J. Mater. Chem. C* **2014**, *2*, 2998.
- [3] Y. Guo, G. Yu, Y. Liu, *Adv. Mater.* **2010**, *22*, 4427.
- [4] X. Zhan, Z. A. Tan, B. Domercq, Z. An, X. Zhang, S. Barlow, Y. Li, D. Zhu, B. Kippelen, S. R. Marder, *J. Am. Chem. Soc.* **2007**, *129*, 7246.
- [5] K. Mazzi, C. Luscombe, *Chem. Soc. Rev.* **2015**, *44*, 78.
- [6] E. Fazio, L. D'Urso, G. Consiglio, A. Giuffrida, G. Compagnini, O. Puglisi, S. Patanè, F. Neri, G. Forte, *J. Phys. Chem. C* **2014**, *118*, 28812.
- [7] G. Forte, L. D'Urso, E. Fazio, S. Patanè, F. Neri, O. Puglisi, G. Compagnini, *Appl. Surf. Sci.* **2013**, *272*, 76.
- [8] W. Li, F. Guo, H. Ling, P. Zhang, M. Yi, L. Wang, D. Wu, L. Xie, W. Huang, *Adv. Sci.* **2017**, *4*, 1700007.
- [9] F. Silvestri, M. J. Prieto, A. Babuji, L. C. Tañase, L. S. Caldas, O. Solomeshch, T. Schmidt, C. Ocal, E. Barrena, *Appl. Mater. Interfaces* **2020**, *12*, 25444.
- [10] T. Sekitani, T. Someya, *Adv. Mater.* **2010**, *22*, 2228.
- [11] O. Inganaš, *Adv. Mater.* **2018**, *30*, 1800388.
- [12] E. K. Lee, M. Y. Lee, C. H. Park, H. R. Lee, J. H. Oh, *Adv. Mater.* **2017**, *29*, 1703638.
- [13] O. Ostroverkhova, *Chem. Rev.* **2016**, *116*, 13279.
- [14] T. Okamoto, M. L. Senatore, M. M. Ling, A. B. Mallik, M. L. Tang, Z. Bao, *Adv. Mater.* **2007**, *19*, 3381.
- [15] G. M. L. Consoli, M. L. Giuffrida, C. Satriano, T. Musumeci, G. Forte, S. Petralia, *Chem. Commun.* **2022**, *58*, 3126.
- [16] G. Consiglio, G. Forte, *Phys. Chem. Chem. Phys.* **2018**, *20*, 29754.
- [17] S. Petralia, G. Forte, M. Zimbone, S. Conoci, *Colloids Surf., B* **2020**, *187*, 110648.
- [18] S. Petralia, T. Barbuzzi, G. Ventimiglia, *Mater. Sci. Eng., C* **2012**, *32*, 848.
- [19] L. Yen-Yi, D. I. Gundlach, S. F. Nelson, T. N. Jackson, *IEEE Trans. Electron Devices* **1997**, *44*, 1325.
- [20] T. W. Kelley, D. V. Muyres, P. F. Baude, T. P. Smith, T. D. Jones, *Mater. Res. Soc. Symp. Proc.* **2003**, *771*, L6.5.1.
- [21] A. Maliakal, K. Raghavachari, H. Katz, E. Chandross, T. Siegrist, *Chem. Mater.* **2004**, *16*, 4980.
- [22] D. Holmes, S. Kumaraswamy, A. J. Matzger, K. P. C. Vollhardt, *Chem. – Eur. J.* **1999**, *5*, 3399.
- [23] T. Siegrist, C. Kloc, J. H. Schön, B. Batlogg, R. C. Haddon, S. Berg, G. A. Thomas, *Angew. Chem. Int. Ed. Engl.* **2001**, *40*(9), 1732.
- [24] R. B. Campbell, J. M. Robertson, J. Trotter, *Acta Crystallogr.* **1961**, *14*, 705.
- [25] M. L. Tiago, J. E. Northrup, S. G. Louie, *Phys. Rev. B* **2003**, *67*, 115212.
- [26] M. L. Tang, J. H. Oh, A. Devi Reichardt, Z. Bao, *J. Am. Chem. Soc.* **2009**, *131*, 3733.
- [27] A. Afzali, C. D. Dimitrakopoulos, T. L. Breen, *J. Am. Chem. Soc.* **2002**, *124*, 8812.
- [28] T. Takahashi, M. Kitamura, B. Shen, K. Nakajima, *J. Am. Chem. Soc.* **2000**, *122*(51), 12876.

- [29] R. Bhatia, D. Wadhawa, G. Gurt, J. Gaur, D. Gupta, J. Os, *Saudi Chem. Soc.* **2019**, 23(7), 925.
- [30] J. E. Anthony, J. S. Brooks, D. L. Eaton, S. R. Parkin, *J. Am. Chem. Soc.* **2001**, 123(38), 9482.
- [31] J. E. Anthony, D. L. Eaton, S. R. Parkin, *Org. Lett.* **2002**, 4(1), 15.
- [32] G. Giri, E. Verploegen, S. C. B. Mannsfeld, S. Atahan-Evrenk, D. H. Kim, S. Yoon Lee, H. A. Becerril, A. Aspuru-Guzik, M. F. Toney, Z. Bao, *Nature* **2011**, 480, 504.
- [33] H. S. Nalwa, *Adv. Mater.* **1993**, 5, 341.
- [34] J. L. Bredas, C. Adant, P. Tackx, A. Persoons, B. M. Pierce, *Chem. Rev.* **1994**, 94, 243.
- [35] M. Zhao, K. Liu, Y. D. Zhang, Q. Wang, Z. G. Li, Y. L. Song, H. L. Zhang, *Mater. Horiz.* **2015**, 2, 619.
- [36] Y. Liu, C. Zhang, R. Wang, B. Zhang, Z. Tan, X. Wang, M. Xiao, *Angewandte* **2015**, 54, 6222.
- [37] I. S. Yahia, S. Alfaify, A. Jilani, M. S. Abdel-wahab, A. A. Al-Ghamdi, M. M. Abutalib, A. Al-Bassam, A. M. El-Naggar, *Appl. Phys. B* **2016**, 122(7), 191.
- [38] G. F. Salem, E. A. A. El-Shazly, A. A. M. Farag, I. S. Yahia, *Optik* **2018**, 174, 221.
- [39] G. Yang, L. Fang, K. Tan, S. Shi, Z. Su, R. Wang, *Organometallics* **2007**, 26, 2082.
- [40] T. Tonami, T. Nagami, K. Okada, W. Yoshida, M. Nakano, *ACS Omega* **2019**, 4, 16181.
- [41] O. Lobanova Griffith, J. E. Anthony, A. G. Jones, D. L. Lichtenberger, *J. Am. Chem. Soc.* **2010**, 132(2), 580.
- [42] I. Muz, M. Kurban, M. Dalkilic, *J. Comput. Electr.* **2020**, 19, 895.
- [43] T. M. Halasinski, D. M. Hudgins, F. Salama, L. J. Allamandola, T. Bally, *J. Phys. Chem. A* **2000**, 104, 7484.
- [44] A. V. Marenich, C. J. Cramer, D. G. Thrular, *J. Phys. Chem. B* **2009**, 113, 6378.
- [45] T. Yanai, D. P. Tew, N. C. Handy, *Chem. Phys. Lett.* **2004**, 393, 51.
- [46] I. Benkyi, E. Tapavicza, H. Fliegl, D. Sundholm, *Phys. Chem. Chem. Phys.* **2019**, 21, 21094.
- [47] W. Fan, D. Tan, W. Q. Deng, *Chem. Phys. Chem.* **2012**, 13, 2051.
- [48] B. Champagne, E. A. Perpete, S. J. A. van Gisbergen, E. J. Baerends, J. G. Snijders, C. Soubra-Ghaoui, K. A. Robins, B. Kirtman, *J. Chem. Phys.* **1998**, 109, 10489.
- [49] P. A. Limacher, K. V. Mikkelsen, H. P. Luthy, *J. Chem. Phys.* **2009**, 130, 194114.
- [50] M. J. Frisch, G. W. Trucks, H. B. Schlegel, G. E. Scuseria, M. A. Robb, J. R. Cheeseman, G. Scalmani, V. Barone, G. A. Petersson, H. Nakatsuji, X. Li, M. Caricato, A. V. Marenich, J. Bloino, B. G. Janesko, R. Gomperts, B. Mennucci, H. P. Hratchian, J. V. Ortiz, A. F. Izmaylov, J. L. Sonnenberg, D. Williams-Young, F. Ding, F. Lipparini, F. Egidi, J. Goings, B. Peng, A. Petrone, T. Henderson, D. Ranasinghe, V. G. Zakrzewski, J. Gao, N. Rega, G. Zheng, W. Liang, M. Hada, M. Ehara, K. Toyota, R. Fukuda, J. Hasegawa, M. Ishida, T. Nakajima, Y. Honda, O. Kitao, H. Nakai, T. Vreven, K. Throssell, J. A. Montgomery, Jr., J. E. Peralta, F. Ogliaro, M. J. Bearpark, J. J. Heyd, E. N. Brothers, K. N. Kudin, V. N. Staroverov, T. A. Keith, R. Kobayashi, J. Normand, K. Raghavachari, A. P. Rendell, J. C. Burant, S. S. Iyengar, J. Tomasi, M. Cossi, J. M. Millam, M. Klene, C. Adamo, R. Cammi, J. W. Ochterski, R. L. Martin, K. Morokuma, O. Farkas, J. B. Foresman, D. J. Fox, Gaussian, Inc., Wallingford CT, **2016**. Gaussian 16 Rev C.01.
- [51] S. Schiefer, M. Huth, A. Dobrinevski, B. Nickel, *J. Am. Chem. Soc.* **2007**, 129(34), 10316.
- [52] P. Dauber-Osguthorpe, V. A. Roberts, D. J. Osguthorpe, J. Wolff, M. Genest, A. T. Hagler, *Struct. Funct. Genet.* **1998**, 4, 31.
- [53] G. Consiglio, S. Failla, C. G. Fortuna, L. D'Urso, G. Forte, *Comput. Theor. Chem.* **2015**, 1067, 1.
- [54] Material Studio package, Material Studio package, BIOVIA, Dassault Systemes, San Diego, USA, **2017**.
- [55] T. Lu, F. Chen, *J. Comput. Chem.* **2012**, 33, 580.
- [56] J. L. Oudar, *J. Chem. Phys.* **1977**, 67, 446.

## SUPPORTING INFORMATION

Additional supporting information can be found online in the Supporting Information section at the end of this article.

**How to cite this article:** S. Petralia, G. Forte, *J Phys Org Chem* **2022**, e4443. <https://doi.org/10.1002/poc.4443>